Hindawi
Wireless Communications and Mobile Computing
Volume 2022, Article ID 8593474, 12 pages
https://doi.org/10.1155/2022/8593474

Research Article

Security Performance Analysis of Relay Networks Based on κ-μ Shadowed Channels with RHIs and CEEs

Jiangfeng Sun,[1] **Xiaohong Wang**,[2] **Yiwei Fang**,[3] **Xinji Tian**,[2] **Mingfu Zhu**,[1] **Jiangtao Ou**,[4] **and Chengyuan Fan**[4]

[1]*The College of Computer Science and Technology, Henan Polytechnic University, Jiaozuo 454003, China*
[2]*The College of Physics and Electronic Information Engineering, Henan Polytechnic University, Jiaozuo 454003, China*
[3]*Wuhan Maritime Communication Research Institute, Wuhan 430079, China*
[4]*AI Sensing Technology, Foshan 528000, China*

Correspondence should be addressed to Xiaohong Wang; wangxiaohonghpu@163.com

Received 13 January 2022; Revised 25 February 2022; Accepted 28 March 2022; Published 13 April 2022

Academic Editor: Zhao Junhui

This paper mainly describes the transmission reliability and physical layer security of multiantenna decode-and-forward relay networks over the κ-μ shadowed fading distribution. We consider the existence of residual hardware impairments (RHIs) and channel estimation errors (CEEs) at the same time. Firstly, we give the network model. On this basis, we analyze the reliability and security by deriving the exact expressions of outage probability (OP) and intercept probability (IP). To further verify and investigate the theoretical derivation, the approximate analysis of OP is obtained under the high signal-to-noise ratio. In addition, we also use an optimized antenna selection technology at the transmitter to improve the security performance. Finally, through the comparative study of theoretical simulation and Monte Carlo simulation results, the factors affecting network transmission and security are acquired. The interesting conclusion is that both RHIs and CEEs can increase OP and decrease IP; that is to say, the existence of RHIs and CEEs can reduce reliability and enhance security.

1. Introduction

With the widespread application of wireless communication technology, physical layer security (PLS) technology is highly concerned by scholars because it can take advantage of channel fading to improve antieavesdropping performance. The PLS was first proposed in [1]. Then, Yang et al. in [2] described that one of the dominating troubles faced by the 5G network is how to ensure the security of wireless data transmission. PLS have been generally studied in different system models, such as cooperative nonorthogonal multiple access (NOMA) systems [3], green communication systems based on relay selection [4], and multihop relay systems [5]. Moreover, Zhu and Yao in [6] also designed a cooperative beamforming scheme to enhance the PLS of cognitive radio networks. The authors of [7] investigated the reliability of quasistatic Rayleigh fading by deriving its outage probability (OP). The authors in [8] proposed a PLS project based on channel precompensation to improve the anti-interference of the polarization shift keying modulation system. Fan et al. in [9] used the relay selection to improve PLS when there are multiple users and multiple eavesdroppers.

In the actual communication process, interference from obstacles or other factors will be encountered inevitably, and the phenomenon that causes the power of the received signals to change with time and position is called channel fading. On account of the rapid development of communication networks, the researches on the transmission and security performances of various models under fading channels have been more and more favored by scholars. The authors in [10] studied the security of the fading channels when there was an eavesdropper in the system model. The authors of [11] explored the channel capacity of multiple-input

multiple-output (MIMO) systems under Rayleigh fading. Zhu et al. in [12] considered the full-duplex decode-and-forward (DF) system in the Rayleigh fading and gave the upper and lower bound expressions of its OP. New closed-form expressions of the strictly positive secrecy capacity (SPSC) and secure outage probability (SOP) over κ-μ fading channels were given in [13]. Badarneh et al. deduced the precise expression of the nth moment of the dual α-μ fading in [14]. And the performance was researched in terms of channel quality estimation index and average channel capacity (ACC). By deriving the precise expressions of average duration of fades (ADF) and probability density function (PDF) for dual Hoyt fading in [15], the authors investigated the statistical characteristics of the fading model of the narrow-band amplify and forward (AF) in this fading environment. In [16], the OP of double shadowed κ-μ fading was analyzed, and the effect of double shadowed on wireless fading channels was discussed. The authors of [17] derived the accurate expressions of PDF and cumulative distribution function (CDF) of amplitude and signal-to-noise ratio (SNR) of multicascade κ-μ fading channels and obtained the closed-form expressions of OP, average symbol error probability (ASEP), and ACC.

In wireless communication networks, cooperative relay technology can improve system reliability, energy efficiency, and system coverage, which has been studied extensively [18–24]. The authors in [18] researched the performance of the double-hop relay system. The application of a full-duplex AF relay system in vehicle-to-vehicle (V2V) was investigated in [19]. Majhi et al. of [20] deduced an accurate expression of the OP of orthogonal frequency division multiplexing (OFDM) relay system. The authors in [21] considered the selection of relay antenna in the V2V communication model using both physical-layer network coding and AF schemes in dual Nakagami-m channels. The OP of the two-way relay DF system under the packet fading channels was investigated in [22]. The authors in [23] studied the influence of the relay selection scheme and the number of relays on the outage performance of cognitive radio networks (CRN) by analyzing the OP. The authors of [24] analyzed the security of relay systems using AF under generalized-K fading.

Due to the time-varying characteristics of the communication state, radio frequency devices will be affected by many factors, such as phase noise and power amplifier nonlinearity. These irreparable hardware impairments (HIs) will distort the signals in transmission, so it is necessary to consider the HIs in a communication system. In addition to the above-mentioned HIs that will threaten the accurate transmission of the signal, the existence of CEEs is also one of the reasons for the mismatch between the expected signal and the actual transmission signal. To make the research more practical, many researchers have considered the influence of transceiver HIs and CEEs on the system during modeling and analysis [25–31], such as cognitive amplification and forwarding multirelay networks [25], beyond fifth-generation Internet of Things collaborative NOMA relay system [26], and ambient backscatter NOMA systems [27]. The authors of [28] described the performance of multiple relay systems when there were both transceiver HIs and CEEs. The authors in [29] studied the influence of RHIs and CEEs on cooperative NOMA systems by analyzing OP and the energy efficiency. The influences of the MIMO system with CEEs, RHIs, and imperfect successive interference cancellation effects on Nakagami-m fading were investigated in [30]. Li et al. of [31] researched the reliability and security performance of cooperative multirelay systems with RHIs and CEEs by deriving and analyzing the accurate expressions of OP and IP.

Through studying the existing fading channels, we found that the newly emerging κ-μ shadowed fading can characterize many fading channels by changing its parameters, such as Rice, Nakagami-m, Rayleigh, and κ-μ. The κ-μ shadowed fading was first proposed in [32]. Due to its composite characteristics, the channels can be applied to many scenarios. As shown in [33], a secure multicast scheme under κ-μ shadowed fading with multiple users and multiple eavesdroppers was studied. Sun et al. in [34] investigated the security performance of the single-input multiple-output relay communication architecture over the κ-μ shadowed distribution by deriving the precise and approximate expressions of SOP and SPSC. The closed-form expressions of the OP and the ASEP of the two-hop multiantenna wireless transmission system based on the AF relay node of the κ-μ shadowed fading system were deduced in [35]. Illi et al. in [36] researched the security of a dual-hop underwater communication system based on the κ-μ shadowed architecture. The authors in [37] studied the performance of the dual-hop autofocus communication network over the κ-μ shadowed fading.

References [10–17] mainly described the research of scholars on wireless fading channel in recent years, [18–24] were aimed at elaborating a widely used cooperative relay technology, [25–31] presented the performance of the system when scholars consider the existence of CEEs and HIs in different models in recent years, and [32–37] described the relevant researches on κ-μ shadowed fading channel in recent years. Synthesizing the above researches, to the author's knowledge, no scholars have studied the effects of RHIs and CEEs with DF under κ-μ shadowed fading. Therefore, we develop this work. First of all, we consider an eavesdropping model with DF relay and study the influence of CEEs and RHIs on the transmission performance and anti-interference ability of the network over κ-μ shadowed fading channels. In addition, to further verify and analyze the theoretical derivation, the high SNR approximate analysis of OP is obtained. Moreover, we also compared the ideal and non-ideal situations

The rest of this article is organized as follows. In Section 2, the statistical characteristics of the system model and the κ-μ shadowed fading are given, and the expressions of each parameter are analyzed when the RHIs and CEEs are considered simultaneously. In Section 3, the antenna selection scheme at the transmitter is given first; then, the precise expressions of OP and IP under ideal and nonideal situations are described. In Section 4, the approximate expressions of high SNR of OP under fixed value and varying function of channel estimation variance are derived. In Section 5, the numerical simulation results are discussed in detail. Section 6 summarizes the article, and the next section is the appendix.

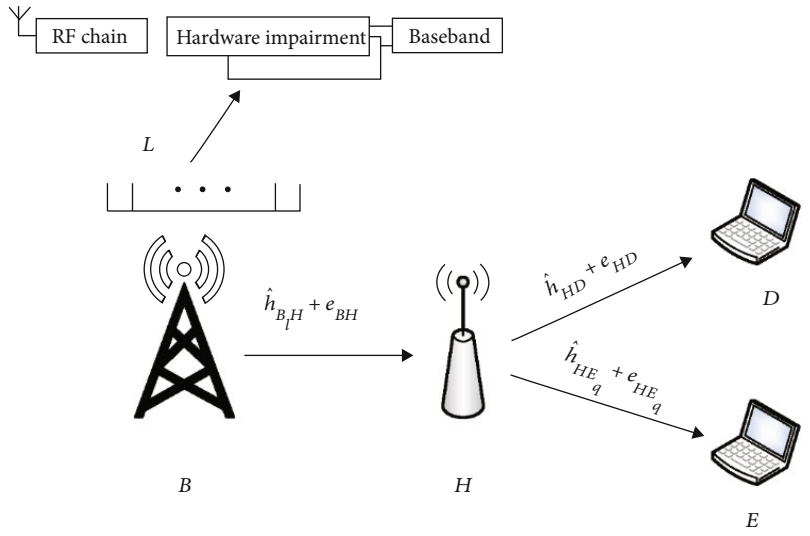

Figure 1: The system model.

2. System Model and Statistical Features

2.1. System Model. In Figure 1, we consider the classic Wyner wiretapping model. The model includes a transmitter (B), a relay (H), a receiver user (D), and an eavesdropper (E). The B is equipped with L antennas $\{B_1, B_1, \cdots, B_l, \cdots, B_L\}$, H and legitimate D have an antenna, and E has Q antennas $\{E_1, E_1, \cdots, E_q, \cdots, E_Q\}$. On account of the existence of the shadowed fading, all signals from the B can only be transmitted to H and cannot be directly sent to D or E. In addition, the information transmission mode at the relay is assumed to be DF.

As can be seen, the communication system of this model is divided into two time slots: (i) B sends the original signals to H; (ii) the H decodes the signals and forwards them to D. To improve the antieavesdropping ability, we have added artificial noise to the model. Since it is difficult to acquire the channel state information (CSI) of all nodes, the effective way to solve this problem is channel estimation which can be divided into three types, including reference signal-based estimation [38], blind estimation [39], and semiblind estimation [40]. The method used in this paper belongs to the first category that uses training sequences to estimate the CSI. According to the method in reference [41], the actual communication channel is expressed as

$$h_{XY} = \widehat{h}_{XY} + e_{XY}. \tag{1}$$

In (1), $XY \in \{B_lH; HD; HE_q\}$, $(1 \le l \le L, 1 \le q \le Q)$, h_{XY} is the channel coefficient, and $\widehat{h}_{XY}$ denotes the channel estimation of h_{XY}. $e_{XY} \sim CN(0, \sigma^2_{e_{XY}})$ represents the CEEs and $\sigma^2_{e_{XY}}$ denotes the estimated variance. We assume two typical conditions: (i) $\sigma^2_{e_{XY}} = M$, where M is a nonnegative value; (ii) $\sigma^2_{e_{XY}} = \Omega/(1 + \delta\rho\Omega)$, where $\Omega, \delta > 0$, and ρ represent the variance of the channel gain, the quality parameter of the CEEs, and the variance of the average SNR, respectively.

2.2. The First Transfer Process. During this course, the signals from B to H are represented as x_{B_lH}, and $E\{|x_{B_lH}|^2\} = 1$. We considered both RHIs and defective CSI, so the information at the H can be described as

$$y_{B_lH} = \left(\widehat{h}_{B_lH} + e_{B_lH}\right)\left(\sqrt{P_B}x_{B_lH} + \eta_{t,B_lH}\right) + \eta_{r,B_lH} + \nu_{B_lH}, \tag{2}$$

where $\widehat{h}_{B_lH}$ represents the channel from the antenna chosen by the B to H. The total transmit power is P, and τ is employed to represent the selected antenna power allocation factor, and $1 - \tau$ indicates the power allocation factor of the unchecked antenna. Here, we employ P_B to indicate the power of the B, then $P_B = \tau P$. x_{B_lH} is the valid signal from B to H, $E\{|x_{B_lH}|^2\} = 1$, and $\nu_{B_lH} \sim CN(0, \sigma^2_{B_lH})$ is the additive white Gaussian noise (AWGN). η_{t,B_lH} and η_{r,B_lH} are, respectively, expressed as the distortion noise caused by RHIs at the transmitting and the receiving terminal.

2.3. The Second Transfer Process. At H, the relay forwards the decoding of the signal to D and E. To improve the antieavesdropping ability, when H transmits information to D and E, the influence of artificial noise is also considered. In the actual communication system, due to the existence of CEEs at D, there will be some artificial noise and residual interference [42–44]. In summary, the information at D and E_q can be written as

$$y_{HD} = \left(\widehat{h}_{HD} + e_{HD}\right)\left(\sqrt{P_H}x_{HD} + \eta_{t,HD}\right) + \eta_{r,HD} + \nu_{HD}, \tag{3}$$

$$y_{HE_q} = \left(\widehat{h}_{HE_q} + e_{HE_q}\right)\left(\sqrt{P_H}x_{HE_q} + \eta_{t,HE_q}\right) + \eta_{r,HE_q} + \nu_{HE_q}, \tag{4}$$

where x_{HD} and x_{HE_q} represent the actual signals transmitted to D and E_q with $E\{|x_{HD}|^2\} = E\{|x_{HE_q}|^2\} = 1$. $x_{J_{HD}}$ and $x_{J_{HE_q}}$ are, respectively, denoted as the signals sent to D and E_q with artificial noise. And $E\{|x_{J_{HD}}|^2\} = E\{|x_{J_{HE_q}}|^2\} = 1$. $\xi_1 \in (0,1)$ and $\xi_2 \in (0,1)$ separately describe the factitious noise quantization coefficients at D and E_q. ν_{HD} and ν_{HE_q}, respectively, represent the composite AWGN with mean value 0 and variance σ^2_{HD} and $\sigma^2_{HE_q}$. P_S and P_J represent the transmit power of relay and factitious noise and $P_B = P_H = P_g$. $\eta_{t,HD}$ and $\eta_{r,HD}$ are, respectively, expressed as the distortion noise caused by RHIs during H to D communication. η_{t,HE_q} and η_{r,HE_q} are, respectively, expressed as the distortion noise caused by RHIs during H to E_q communication. As mentioned in [45], the distortion noise can be written as

$$\eta_t \sim CN\left(0, f_t^2 P_g\right), \eta_r \sim CN\left(0, f_r^2 P_g |h|^2\right). \tag{5}$$

The distortion noise was regarded as the product of η_t, η_r, and h. For an achievable channel h, the composite distortion power at the receiving terminal can be described as

$$E_{\eta_t,\eta_r}\left\{|h\eta_t + \eta_r|^2\right\} = P_g|h|^2\left(f_t^2 + f_r^2\right) = P_g\left|\widehat{h} + e\right|^2\left(f_t^2 + f_r^2\right). \tag{6}$$

From (6), we can get that power only rests with the p_g and the $|\widehat{h}_{XY}|^2$. Where $f_{XY} = \sqrt{f_{t,XY}^2 + f_{r,XY}^2}$, the messages at H, D, and E_q were described as

$$y_{B_lH} = \left(\widehat{h}_{B_lH} + e_{B_lH}\right)\left(\sqrt{P_B}x_{B_lH} + \eta_{B_lH}\right) + \nu_{B_lH}, \tag{7}$$

$$y_{HD} = \left(\widehat{h}_{HD} + e_{HD}\right)\left(\sqrt{P_H}x_{HD} + \sqrt{\xi_1 P_J}x_{J_{HD}} + \eta_{HD}\right) + \nu_{HD}, \tag{8}$$

$$y_{HE_q} = \left(\widehat{h}_{HE_q} + e_{HE_q}\right)\left(\sqrt{P_H}x_{HE_q} + \sqrt{\xi_2 P_J}x_{J_{HE_q}} + \eta_{HE_q}\right) + \nu_{HE_q}, \tag{9}$$

where the comprehensive distortion noises from RHIs at $B_l \longrightarrow H$, $H \longrightarrow D$, and $H \longrightarrow E_q$ are, respectively, expressed as $\eta_{B_lH} \sim CN(0, f^2_{B_lH}P_B)$, $\eta_{HD} \sim CN(0, f^2_{HD}P_H)$, and $\eta_{HE_q} \sim CN(0, f^2_{HE_q}P_H)$. Besides, $f_{B_lH} = \sqrt{f^2_{t,B_lH} + f^2_{r,B_lH}}$, $f_{HD} = \sqrt{f^2_{t,HD} + f^2_{r,HD}}$, and $f_{HE_q} = \sqrt{f^2_{t,HE_q} + f^2_{r,HE_q}}$.

The signal-to-interference-plus-noise ratios (SINRs) of $B_l \longrightarrow H$, $H \longrightarrow D$, and $H \longrightarrow E_q$ are given as

$$\gamma_{B_lH} = \frac{\rho_{B_lH}\left|\widehat{h}_{B_lH}\right|^2}{\rho_{B_lH}\left(\sigma^2_{e_{B_lH}} + \left|\widehat{h}_{B_lH}\right|^2 f^2_{B_lH} + \sigma^2_{e_{B_lH}} f^2_{B_lH}\right) + 1}, \tag{10}$$

$$\gamma_{HD} = \frac{\rho_{HD}\left|\widehat{h}_{HD}\right|^2}{\rho_{HD}\sigma^2_{e_{HD}} + \left(\xi_1 P_J/\sigma^2_{HD} + \rho_{HD}f^2_{HD}\right)\left(\left|\widehat{h}_{HD}\right|^2 + \sigma^2_{e_{HD}}\right) + 1}, \tag{11}$$

$$\gamma_{HE_q} = \frac{\rho_{HE_q}\left|\widehat{h}_{HE_q}\right|^2}{\rho_{HE_q}\sigma^2_{e_{HE_q}} + \left(\xi_2 P_J/\sigma^2_{HE_q} + \rho_{HE_q}f^2_{HE_q}\right)\left(\left|\widehat{h}_{HE_q}\right|^2 + \sigma^2_{e_{HE_q}}\right) + 1}, \tag{12}$$

where $\rho_{B_lH} = P_B/\sigma^2_{B_lH}$, $\rho_{HD} = P_H/\sigma^2_{HD}$, and $\rho_{HE_q} = P_H/\sigma^2_{HE_q}$.

2.4. Statistical Features. In the model, we consider the widely applied κ-μ shadowed fading, and the PDF of the channel gain has been given in [46] as

$$\begin{aligned} f_{|\widehat{h}_{XY}|^2}(x) = {} & \frac{{m_{XY}}^{m_{XY}}(1+\kappa_{XY})^{\mu_{XY}}{\mu_{XY}}^{\mu_{XY}}}{\Gamma(\mu_{XY})(m_{XY}+\kappa_{XY}\mu_{XY})^{m_{XY}}\psi_{XY}} \\ & \cdot \exp\left(-\frac{x(1+\kappa_{XY})\mu_{XY}}{\psi_{XY}}\right) \times \left(\frac{x}{\psi_{XY}}\right)^{\mu_{XY}-1} {}_1F_1 \\ & \cdot \left(m_{XY}; \mu_{XY}; \frac{\mu^2_{XY}\kappa_{XY}(1+\kappa_{XY})x}{\psi_{XY}(m_{XY}+\kappa_{XY}\mu_{XY})}\right). \end{aligned} \tag{13}$$

After some mathematical operations, the CDF expression of the channel gain can be obtained as

$$\begin{aligned} F_{|\widehat{h}_{XY}|^2}(x) = {} & \left(\frac{m_{XY}+\kappa_{XY}\mu_{XY}}{m_{XY}}\right)^{-m_{XY}} \frac{1}{\Gamma(\mu_{XY})}\sum_{i=1}^{\infty}\frac{(m_{XY})_i}{(\mu_{XY})_i i!} \\ & \cdot \left(\frac{m_{XY}\kappa_{XY}\mu_{XY}}{(m_{XY}+\kappa_{XY}\mu_{XY})m_{XY}}\right)^i \times (\mu_{XY}+i-1)! \\ & \cdot \left\{1 - \sum_{s=0}^{\mu_{XY}+i-1}\frac{x^s}{s!}\left[\frac{(1+\kappa_{XY})\mu_{XY}}{\psi_{XY}}\right]^s \right. \\ & \left. \cdot \exp\left(-\frac{(1+\kappa_{XY})\mu_{XY}}{\psi_{XY}}x\right)\right\}. \end{aligned} \tag{14}$$

The meanings of κ, m, and μ in (13) and (14) are all channel parameters, where m is the shaping parameter of Nakagami-m fading, and $\mu > 0$ is related to the number of received signal groups. $\kappa = d^2/2\mu\sigma^2$ is a positive number, d^2 represents the total power of the dominating constituent, and $2\mu\sigma^2$ is the total power of the scattered wave. $\psi = E\{|\widehat{h}_{XY}|^2\}$, and $|\widehat{h}_{XY}|$ indicates the amplitude of the channel. The capacity formula of the Shannon theorem is defined as

$$C = \frac{1}{2}\log_2\{1+\gamma\}. \tag{15}$$

According to (10) and (11), we can get the expression of the instantaneous channel capacity of $B \longrightarrow H$ and $H \longrightarrow D$

as

$$C_{BH} = \frac{1}{2}\log_2\left\{1 + \frac{\rho_{BH}\left|\widehat{h}_{BH}\right|^2}{\rho_{BH}\left(\sigma^2_{e_{BH}} + \left|\widehat{h}_{BH}\right|^2 f^2_{BH} + \sigma^2_{e_{BH}} f^2_{BH}\right) + 1}\right\}, \tag{16}$$

$$C_{HD} = \frac{1}{2}\log_2\left\{1 + \frac{\rho_{HD}\left|\widehat{h}_{HD}\right|^2}{\rho_{HD}\sigma^2_{e_{HD}} + \left(\xi_1 P_J/\sigma^2_{HD} + \rho_{HD} f^2_{HD}\right)\left(\left|\widehat{h}_{HD}\right|^2 + \sigma^2_{e_{HD}}\right) + 1}\right\}. \tag{17}$$

The eavesdropper employs multiple relay combining (MRC) algorithm to intercept legal information; the SINR at $H \longrightarrow E$ is

$$\gamma_{HE} = \sum_{q=1}^{Q} \gamma_{HE_q}. \tag{18}$$

The SINR of $H \longrightarrow E$ is expressed as

$$\gamma_{HE} = Q\gamma_{HE_q}. \tag{19}$$

So we can get the instantaneous capacity of $H \longrightarrow E$ as

$$C_{HE} = \frac{1}{2}\log_2\left\{1 + \frac{Q\rho_{HE_q}\left|\widehat{h}_{HE_q}\right|^2}{\rho_{HE_q}\sigma^2_{e_{HE_q}} + \left(\xi_2 P_J/\sigma^2_{HE_q} + \rho_{HE_q} f^2_{HE_q}\right)\left(\left|\widehat{h}_{HE_q}\right|^2 + \sigma^2_{e_{HE_q}}\right) + 1}\right\}. \tag{20}$$

3. Performance Analysis of Outage Probability (OP) and Intercept Probability (IP)

To improve the performance of the communication systems, we use the optimal transmit antenna selection (OTAS) strategy at the transmitter with multiple antennas and deduce the precise expressions of OP and IP to analyze its reliability and security.

3.1. OP Analysis. In this section, we discuss the transmission performance of multiantenna cooperative communication systems in the existence of RHIs and CEEs from the perspective of OP.

3.2. Outage Probability. The OP of the system model can be indicated as

$$P_{\text{out}} = \Pr\{C_{XY} < R_s\}, \tag{21}$$

where the target threshold is R_s.

Under the premise of CEEs and RHIs, using the OTAS protocol, the channel gain containing the estimation error can be obtained as

$$\left|\widehat{h}_{BH}\right| = \max_{1\le l\le L}\left\{\widehat{h}_{B_l H}\right\}. \tag{22}$$

The CDF of the channel gain during $B_l \longrightarrow H$ transmission is written as

$$\begin{aligned} F_{\left|\widehat{h}_{XY}\right|^2}(x) = \Bigg\{ & \left(\frac{m_{XY} + \kappa_{XY}\mu_{XY}}{m_{XY}}\right)^{-m_{XY}} \frac{1}{\Gamma(\mu_{XY})}\sum_{i=1}^{\infty}\frac{(m_{XY})_i}{(\mu_{XY})_i i!} \\ & \times (\mu_{XY} + i - 1)! \times \left(\frac{m_{XY}\kappa_{XY}\mu_{XY}}{(m_{XY} + \kappa_{XY}\mu_{XY})m_{XY}}\right)^i \\ & \cdot \left\{1 - \sum_{s=0}^{\mu_{XY}+i-1}\frac{x^s}{s!}\left[\frac{(1+\kappa_{XY})\mu_{XY}}{\psi_{XY}}\right]^s \right. \\ & \left. \cdot \exp\left(-\frac{(1+\kappa_{XY})\mu_{XY}}{\psi_{XY}}x\right)\right\}\Bigg\}^L. \end{aligned} \tag{23}$$

With the DF algorithm, the channel capacity in the information transmission of $B_l \longrightarrow H$ and $H \longrightarrow D$ is expressed as

$$C_H = \min\left(C_{BH}, C_{HD}\right). \tag{24}$$

Through the above analysis, in the following theorem, we will research the exact expression of the OP of the κ-μ shadowed fading with RHIs and CEEs.

Theorem 1. *For κ-μ shadowed fading, the accurate expressions of OP for two scenes are expressed as follows:*

(1) Nonideal condition (with RHIs and CEEs)

$$P^{ni}_{out} = I_1 + I_2 - I_1 I_2. \tag{25}$$

To ensure that OP is not zero, we set $1 - \Theta f^2_{BH} > 0$ and $\rho_{HD} - \Theta(\xi_1 P_J/\sigma^2_{HD} + f^2_{HD}\rho_{HD}) > 0$. I_1 and I_2 correspond to equations (35) and (36) in the appendix, respectively.

(2) Ideal condition ($f_{BH} = f_{HD} = 0$ and $\sigma^2_{e_{BH}} = \kappa^2_{e_{HD}} = 0$)

$$\begin{aligned} P^{id}_{out} = \Bigg\{ & \left(\frac{m_{BH} + \kappa_{BH}\mu_{BH}}{m_{BH}}\right)^{-m_{BH}} \frac{1}{\Gamma(\mu_{BH})}\sum_{i=1}^{\infty}\frac{(m_{BH})_i}{(\mu_{BH})_i i!} \\ & \cdot (\mu_{BH} + i - 1)!\left(\frac{m_{BH}\kappa_{BH}\mu_{BH}}{(m_{BH} + \kappa_{BH}\mu_{BH})m_{BH}}\right)^i \times \left\{1 - \sum_{s=0}^{\mu_{BH}+i-1}\frac{\varphi_3^s}{s!}\left[\frac{(1+\kappa_{BH})\mu_{BH}}{\psi_{BH}}\right]^s \right. \\ & \left. \cdot \exp\left(-\frac{(1+\kappa_{BH})\mu_{BH}}{\psi_{BH}}\varphi_3\right)\right\}\Bigg\}^L + \Bigg\{\left(\frac{m_{HD} + \kappa_{HD}\mu_{HD}}{m_{HD}}\right)^{-m_{HD}} \\ & \cdot \frac{1}{\Gamma(\mu_{HD})}\sum_{i=1}^{\infty}\frac{(m_{HD})_i}{(\mu_{HD})_i i!}(\mu_{HD} + i - 1)!\left(\frac{m_{HD}\kappa_{HD}\mu_{HD}}{(m_{HD} + \kappa_{HD}\mu_{HD})m_{HD}}\right)^i \\ & \times \left\{1 - \sum_{s=0}^{\mu_{HD}+i-1}\frac{\varphi_4^s}{s!}\left[\frac{(1+\kappa_{HD})\mu_{HD}}{\psi_{HD}}\right]^s \exp\left(-\frac{(1+\kappa_{HD})\mu_{HD}}{\psi_{HD}}\varphi_4\right)\right\}\Bigg\} \\ & - \Bigg\{\left(\frac{m_{BH} + \kappa_{BH}\mu_{BH}}{m_{BH}}\right)^{-m_{BH}} \frac{1}{\Gamma(\mu_{BH})}\sum_{i=1}^{\infty}\frac{(m_{BH})_i}{(\mu_{BH})_i i!}(\mu_{BH} + i - 1)! \\ & \cdot \left(\frac{m_{BH}\kappa_{BH}\mu_{BH}}{(m_{BH} + \kappa_{BH}\mu_{BH})m_{BH}}\right)^i \times \left\{1 - \sum_{s=0}^{\mu_{BH}+i-1}\frac{\varphi_3^s}{s!}\left[\frac{(1+\kappa_{BH})\mu_{BH}}{\psi_{BH}}\right]^s \right. \\ & \left. \cdot \exp\left(-\frac{(1+\kappa_{BH})\mu_{BH}}{\psi_{BH}}\varphi_3\right)\right\}^L \times \left\{\left(\frac{m_{HD} + \kappa_{HD}\mu_{HD}}{m_{HD}}\right)^{-m_{HD}} \right. \\ & \cdot \frac{1}{\Gamma(\mu_{HD})}\sum_{i=1}^{\infty}\frac{(m_{HD})_i}{(\mu_{HD})_i i!}(\mu_{HD} + i - 1)!\left(\frac{m_{HD}\kappa_{HD}\mu_{HD}}{(m_{HD} + \kappa_{HD}\mu_{HD})m_{HD}}\right)^i \\ & \left. \times \left\{1 - \sum_{s=0}^{\mu_{HD}+i-1}\frac{\varphi_4^s}{s!}\left[\frac{(1+\kappa_{HD})\mu_{HD}}{\psi_{HD}}\right]^s \exp\left(-\frac{(1+\kappa_{HD})\mu_{HD}}{\psi_{HD}}\varphi_4\right)\right\}\right\}, \end{aligned} \tag{26}$$

where $\varphi_3 = \Theta/\rho_{BH}$ and $\varphi_4 = \Theta/(\rho_{BH} - \Theta\xi_1 P_J/\sigma^2_{HD})$.

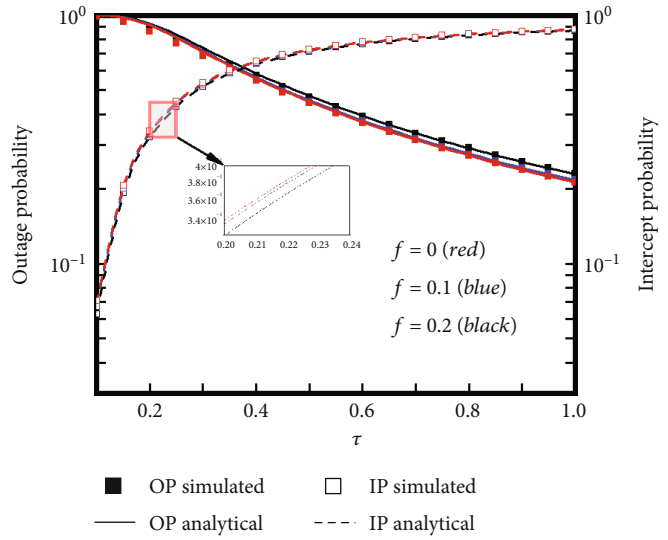

Figure 2: OP and IP versus τ for different f ($\{\xi_1, \xi_2\} = \{0.05, 0.95\}$, $P = 5$ dB, $\sigma_e^2 = 0.1$, $\kappa = 1$, $m = 2$, $\mu = 2$, $L = 2$, and $Q = 2$).

Proof. See Appendix A. □

3.3. IP Analysis. IP means the probability that the capacity of the eavesdropping channel is greater than R_S, which is written as

$$P_{\text{int}} = \Pr\{C_{HE} > R_s\}. \tag{27}$$

For the precise expressions of IP under the κ-μ shadowed fading, the two scenes will be given below.

3.4. Nonideal Condition. Substituting (20) into (27), we obtain

$$P_{\text{int},i.i.d}^{\text{ni}} = \Pr\left\{\frac{Q\rho_{HE_q}\left|\widehat{h}_{HE_q}\right|^2}{\rho_{HE_q}\sigma_{e_{HE_q}}^2 + \left(\xi_2 P_J/\sigma_{HE_q}^2 + \rho_{HE_q} f_{HE_q}^2\right)\left(\left|\widehat{h}_{HE_q}\right|^2 + \sigma_{e_{HE_q}}^2\right) + 1} > \Theta\right\} = 1 - F_{\left|\widehat{h}_{HE_q}\right|^2}(\varphi_5). \tag{28}$$

where $\varphi_5 = (\Xi[\sigma_{e_{HE_q}}^2(\rho_{HE_q} + \xi_2 P_J/\sigma_{HE_q}^2 + \rho_{HE_q} f_{HE_q}^2) + 1])/(\rho_{HE_q} - \Xi(\xi_2 P_J/\sigma_{HE_q}^2 + \rho_{HE_q} f_{HE_q}^2))$, $\Theta = 2^{2R_S} - 1$, and $\Xi = \Theta/Q$. Substituting (14) into (28), we can get the exact expression of OP as

$$P_{\text{int},i.i.d}^{\text{ni}} = 1 - \left(\frac{m_{HE_q} + \kappa_{HE_q}\mu_{HE_q}}{m_{HE_q}}\right)^{-m_{HE_q}} \frac{1}{\Gamma\left(\mu_{HE_q}\right)} \sum_{i=1}^{\infty} \frac{\left(m_{HE_q}\right)_i}{\left(\mu_{HE_q}\right)_i i!} \cdot \left(\frac{m_{HE_q}\kappa_{HE_q}\mu_{HE_q}}{\left(m_{HE_q} + \kappa_{HE_q}\mu_{HE_q}\right)m_{HE_q}}\right)^i \times \left(\mu_{HE_q} + i - 1\right)! \cdot \left\{1 - \sum_{s=0}^{\mu_{HE_q}+i-1} \frac{\varphi_5^s}{s!}\left[\frac{\left(1+\kappa_{HE_q}\right)\mu_{HE_q}}{\psi_{HE_q}}\right]^s \exp\left(-\frac{\left(1+\kappa_{HE_q}\right)\mu_{HE_q}}{\psi_{HE_q}}\varphi_5\right)\right\}. \tag{29}$$

where $\Xi < (\rho_{HE_q}\sigma_{HE_q}^2)/\xi_2 P_J$.

3.5. Ideal Condition. Similar to the derivation of (29), we obtain

$$P_{\text{int}}^{id} = 1 - \left(\frac{m_{HE_q} + \kappa_{HE_q}\mu_{HE_q}}{m_{HE_q}}\right)^{-m_{HE_q}} \frac{1}{\Gamma\left(\mu_{HE_q}\right)} \sum_{i=1}^{\infty} \frac{\left(m_{HE_q}\right)_i}{\left(\mu_{HE_q}\right)_i i!} \cdot \left(\frac{m_{HE_q}\kappa_{HE_q}\mu_{HE_q}}{\left(m_{HE_q} + \kappa_{HE_q}\mu_{HE_q}\right)m_{HE_q}}\right)^i \times \left(\mu_{HE_q} + i - 1\right)! \cdot \left\{1 - \sum_{s=0}^{\mu_{HE_q}+i-1} \frac{\varphi_6^s}{s!}\left[\frac{\left(1+\kappa_{HE_q}\right)\mu_{HE_q}}{\psi_{HE_q}}\right]^s \exp\left(-\frac{\left(1+\kappa_{HE_q}\right)\mu_{HE_q}}{\psi_{HE_q}}\varphi_6\right)\right\}, \tag{30}$$

where $\varphi_6 = \Xi/(\rho_{HE_q} - \Xi\xi_2 P_J/\sigma_{HE_q}^2)$, $\Theta = 2^{2R_S} - 1$, and $\Xi = \Theta/Q$ and we set $\Xi < (\rho_{HE_q}\sigma_{HE_q}^2)/\xi_2 P_J$.

4. Asymptotic Analysis

To further verify and investigate the theoretical derivation, we give the asymptotic analysis of the high SNR approximation of OP. It can be divided into the following two conditions: nonideal case and ideal case.

Theorem 2. *The precise expressions of the asymptotic analysis of the high SNR approximation of OP are as follows:*

(1) Nonideal case

When $\sigma_{e_{XY}}^2 = \Omega/(1 + \delta\rho\Omega)$, equation (42) can be obtained from Appendix B. When $\sigma_{e_{XY}}^2 = a$,

$$P_{out}^{\infty,ni2} = I_5 + I_6 - I_5 I_6, \tag{31}$$

where a is a constant, $1 - \Theta f_{BH}^2 > 0$, and $1 - \Theta\xi_1/2 - \Theta f_{HD}^2 > 0$.

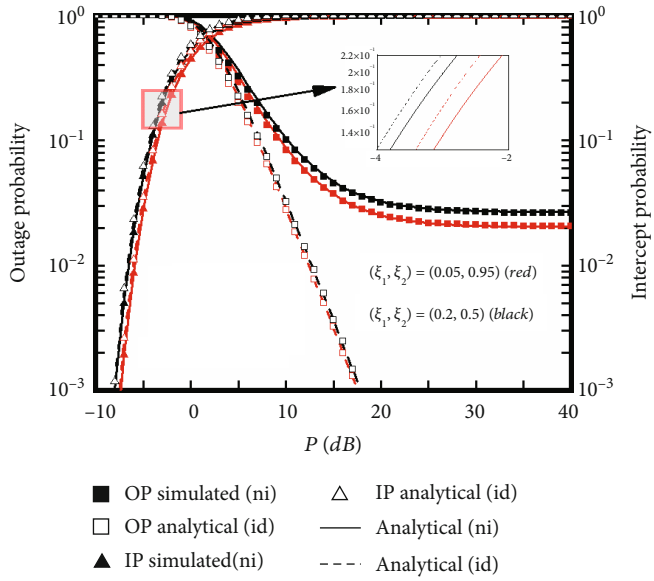

FIGURE 3: OP and IP versus P for different $\{\xi_1, \xi_2\}$ ($L = 2$, $\kappa = 1$, $m = 2$, $\mu = 2$, $\tau = 0.8$, and $Q = 2$).

(2) Ideal case

$$P_{out}^{\infty,id} = I_7 + I_8 - I_7 I_8. \tag{32}$$

Proof. See Appendix B. □

5. Numerical Analysis

In this section, we exhibit the comparison charts between theoretical derivations and Monte Carlo simulations in Figures 2–7. As can be seen from the graphs, the numerical results coincide well with the simulation, which confirms the validity of the deduced results. In the simulation, our parameters are set as follows: $\kappa_{XY} = \kappa$, $m_{XY} = m$, $\mu_{XY} = \mu$, $R_s = 0.5$, $P_B = P_H = P_g$, $P_J = P_B/2$, $\sigma^2_{e_{XY}} = \sigma_e^2$, $\sigma^2_{XY} = 1$, and $\psi_{XY} = 1$. It should be noted that although the theoretical formulas of IP and op contain infinite series, it will not affect the simulation results, because the theoretical formulas will converge when the number of cycles is greater than 45.

Figure 2 describes the variation of OP and IP with the power distribution factor τ and distortion noise f. It can be concluded that as τ increases, OP gradually becomes smaller, while IP continues to rise. And the increase of the distortion noise parameter will reduce the reliability and improve the antieavesdropping ability.

Figure 3 illustrates the changes of OP and IP with transmit power under different artificial quantization coefficients. Both ideal situations ($\sigma_e^2 = 0$, $f = 0$) and nonideal situations ($\sigma_e^2 = 0.1$, $f = 0.1$) are considered. It can be seen that as ξ_1 augments, OP gradually aggrandizes, and the reliability of the system decreases. And due to distortion, the value of OP under ideal conditions is always lower than that with RHIs. In addition, increasing the value of ξ_2 will raise the IP, which means that the security of the channel will be reduced.

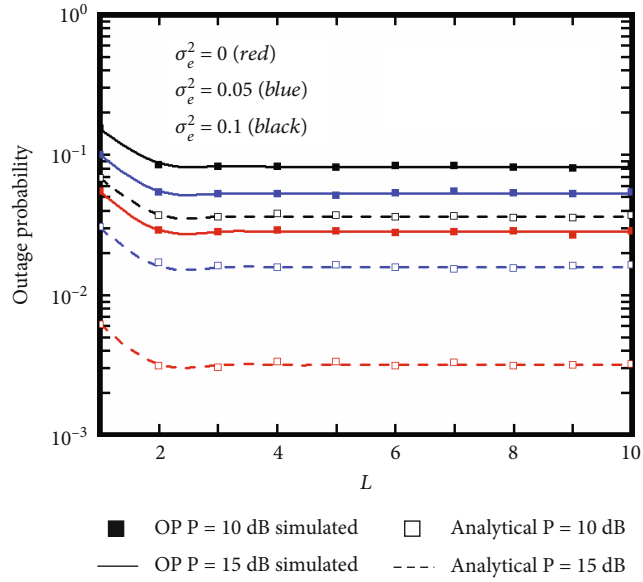

FIGURE 4: OP and IP versus L for different σ_e^2 and P ($\{\xi_1, \xi_2\} = \{0.05, 0.95\}$, $f = 0.1$, $\kappa = 1$, $m = 2$, $\mu = 2$, and $\tau = 0.8$).

Figure 4 plots the impact of different antenna numbers L and CEEs on OP. We clearly find that the increase of transmission power can enhance the transmission performance, while the augment of CEEs will impair the reliability. When the number of antennas is less than 4 dB, the OP decreases as the number of antennas adds. When L is greater than 4 dB, the OP changes less, which shows that the application of OTAS to improve the reliability of the system is more suitable when the number of antennas is small.

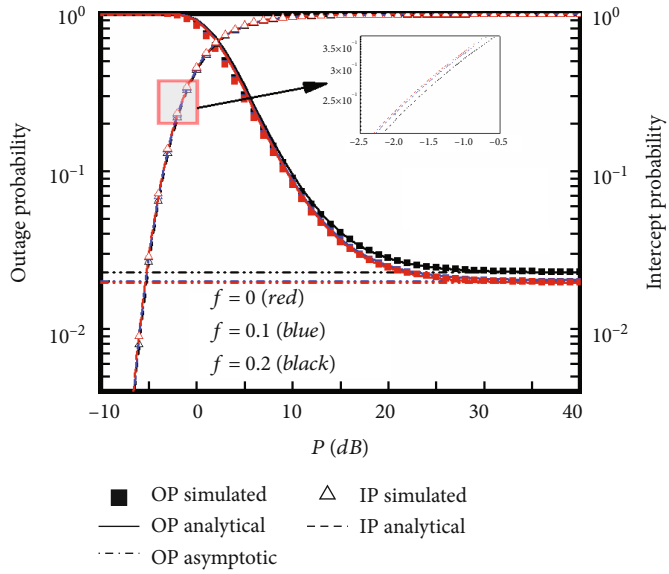

FIGURE 5: OP and IP versus P for different f ($\{\xi_1, \xi_2\} = \{0.05, 0.95\}$, $\tau = 0.8$, $\sigma_e^2 = 0.1$, $f = \{0, 0.1, 0.2\}$, $\kappa = 1$, $m = 2$, $\mu = 2$, $L = 2$, and $Q = 2$).

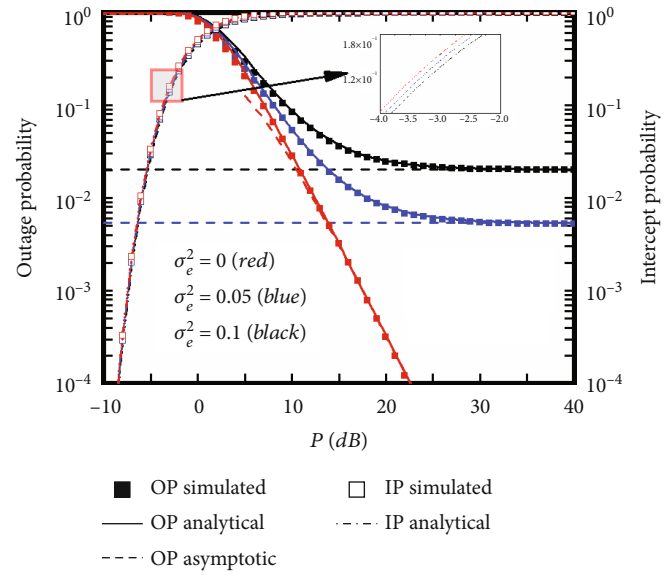

FIGURE 6: OP and IP versus P for different σ_e^2 ($\{\xi_1, \xi_2\} = \{0.05, 0.95\}$, $\tau = 0.8$, $L = 2$, $\kappa = 1$, $m = 2$, $\mu = 2$, $Q = 2$, and $f = 0.1$).

Figure 5 presents the variation of OP and IP with transmission power when RHIs and CEEs exist at the same time. The figure shows that with the increases of f, OP increases while IP decreases. The results illustrate that RHIs are detrimental to the reliability of the system. And OP has an error floor under nonideal conditions. In addition, there is an optimal transmission power, which can balance the security and reliability in the communication process.

Figure 6 illustrates the change of OP and IP with the transmit power under different CEE conditions. The approximate curves in Figure 6 are drawn based on (31) and (32). We can see that in nonideal situations, with the increase of σ_e^2, the reliability of the channel decreases and there exists an error floor. And the value of OP under the nonideal case is always greater than under the ideal case. In addition, compared with OP, CEEs have less impact on IP. This manifests that CEEs play an important role in the reliability but has little impact on the security.

Figure 7 plots the variation of OP under the conditions of different antenna numbers L and parameters μ. In this simulation, we set an ideal case ($\sigma_e^2 = 0$, $f = 0$) and a nonideal case ($\sigma_e^2 = 0.1$, $f = 0.1$). It can be concluded that due to the existence of fixed CEEs, there exists an error floor independent of transmission power under nonideal condition. And because of the existence of CEEs and RHIs, the nonideal situation of OP has been worse than the ideal situation. At the same time, we can see that the augment of L and μ can make the system more reliable.

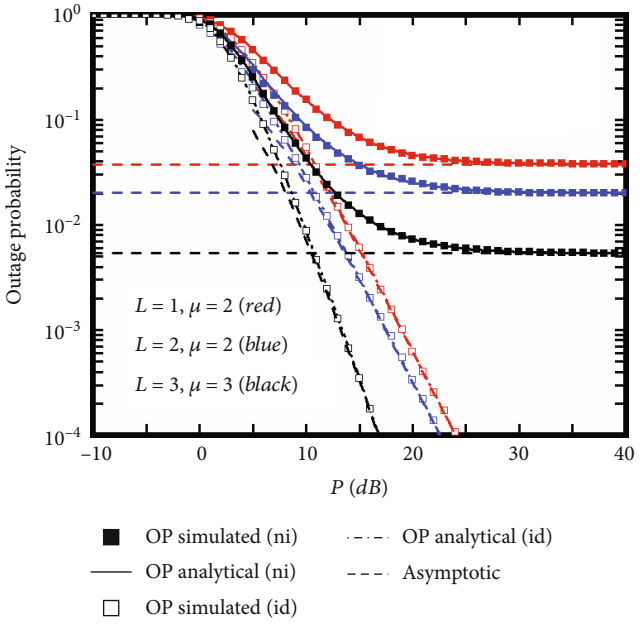

FIGURE 7: OP versus P for different L and μ ($\{\xi_1, \xi_2\} = \{0.05, 0.95\}$, $\tau = 0.8$, $\kappa = 1$, $m = 2$, $L = \{1, 2\}$, and $\mu = \{2, 3\}$).

6. Conclusion

This paper mainly studies the influence over the κ-μ shadowed fading when RHIs and CEEs exist simultaneously. Meanwhile, we used the multiantenna selection scheme on the transmitting terminal and discussed the multiantenna receiving technology on the eavesdropping transmitting terminal. In addition, we employed the DF method to transmit the destination signal and then verified the correctness of the derivation through simulation We discover that large f, large ξ, large σ_e^2, and small L can reduce the reliability. In addition, small ξ, large f, and large σ_e^2 can improve the anti-eavesdropping ability on the κ-μ shadowed network. Finally, it is concluded that RHIs and CEEs can reduce the reliability and enhance its security, because RHIs and CEEs often appear in the practical communication network. It is very meaningful to do performance analysis on this premise. As an extension of this work, we will study the scenario of multiple base stations and multiple receivers with different relay protocols.

Appendix

A. The Proof of Theorem 1

Combining (21) and (24), the expression of OP can be obtained as

$$\begin{aligned} P_{\text{out}} &= \Pr\left\{\min\left(C_{BH,}C_{HD}\right) < R_S\right\} = 1 - \Pr\left\{\min\left(C_{BH,}C_{HD}\right) > R_S\right\} \\ &= \Pr\left\{C_{BH} < R_S\right\} + \Pr\left\{C_{HD} < R_S\right\} \\ &\quad - \Pr\left\{C_{BH} < R_S\right\} \Pr\left\{C_{HD} < R_S\right\} = I_1 + I_2 - I_1 I_2. \end{aligned} \tag{33}$$

In the following process of solving the closed-form expressions of I_1 and I_2, we set $\Theta = 2^{2R_S} - 1$. Then, we substitute (16) into (33) and obtain

$$\begin{aligned} I_1 &= \Pr\left\{\frac{1}{2}\log_2\left(1 + \frac{\rho_{BH}\left|\widehat{h}_{BH}\right|^2}{\rho_{BH}\left(\sigma_{e_{BH}}^2 + \left|\widehat{h}_{BH}\right|^2 f_{BH}^2 + \sigma_{e_{BH}}^2 f_{BH}^2\right) + 1}\right) < R_S\right\} \\ &= \Pr\left\{\left|\widehat{h}_{BH}\right|^2 < \frac{\Theta\rho_{BH}\sigma_{e_{BH}}^2\left(1 + f_{BH}^2\right) + \Theta}{\rho_{BH}\left(1 - \Theta f_{BH}^2\right)}\right\}, \end{aligned} \tag{34}$$

where we set $\varphi_1 = (\Theta\rho_{BH}\sigma_{e_{BH}}^2(1 + f_{BH}^2) + \Theta)/(\rho_{BH}(1 - \Theta f_{BH}^2))$. Finally, substituting (23) into (34), we get the exact expression of I_1 as

$$\begin{aligned} I_1 = \Pr\left\{\left|\widehat{h}_{BH}\right|^2 < \varphi_1\right\} &= \left\{\left(\frac{m_{BH} + \kappa_{BH}\mu_{BH}}{m_{BH}}\right)^{-m_{BH}} \frac{1}{\Gamma(\mu_{BH})}\right. \\ &\cdot \sum_{i=1}^{\infty} \frac{(m_{BH})_i}{(\mu_{BH})_i i!}\left(\frac{m_{BH}\kappa_{BH}\mu_{BH}}{(m_{BH} + \kappa_{BH}\mu_{BH})m_{BH}}\right)^i \times (\mu_{BH} + i - 1)! \\ &\left.\cdot \left\{1 - \sum_{s=0}^{\mu_{BH}+i-1} \frac{\varphi_1^{\,s}}{s!}\left[\frac{(1 + \kappa_{BH})\mu_{BH}}{\psi_{BH}}\right]^s \exp\left(-\frac{(1 + \kappa_{BH})\mu_{BH}}{\psi_{BH}}\varphi_1\right)\right\}\right\}^L. \end{aligned} \tag{35}$$

Similar to the method of solving I_1, we substitute (24) into (33) to gain formula (36), and then, we combine (14) and (36) to get the exact expression of I_2 as

$$\begin{aligned} I_2 &= \Pr\left\{\frac{\rho_{HD}\left|\widehat{h}_{HD}\right|^2}{\rho_{HD}\sigma_{e_{HD}}^2 + \left(\xi_1 P_J/\sigma_{HD}^2 + \rho_{HD} f_{HD}^2\right)\left(\left|\widehat{h}_{HD}\right|^2 + \sigma_{e_{HD}}^2\right) + 1} < \Theta\right\} \\ &= \Pr\left\{\left|\widehat{h}_{HD}\right|^2 < \frac{\Theta\left[\sigma_{e_{HD}}^2\left(\rho_{HD} + \xi_1 P_J/\sigma_{HD}^2 + \rho_{HD} f_{HD}^2\right) + 1\right]}{\rho_{HD} - \Theta\left(\xi_1 P_J/\sigma_{HD}^2 + \rho_{HD} f_{HD}^2\right)}\right\}, \end{aligned} \tag{36}$$

where we set $\varphi_2 = (\Theta[\sigma_{e_{HD}}^2(\rho_{HD} + \xi_1 P_J/\sigma_{HD}^2 + \rho_{HD} f_{HD}^2) + 1])/(\rho_{HD} - \Theta(\xi_1 P_J/\sigma_{HD}^2 + \rho_{HD} f_{HD}^2))$. After further simplification, I_2 can be expressed as

$$\begin{aligned} I_2 = \Pr\left\{\left|\widehat{h}_{HD}\right|^2 < \varphi_2\right\} &= F_{\left|\widehat{h}_{HD}\right|^2}(\varphi_2) \\ &= \left\{\left(\frac{m_{HD} + \kappa_{HD}\mu_{HD}}{m_{HD}}\right)^{-m_{HD}} \frac{1}{\Gamma(\mu_{HD})} \sum_{i=1}^{\infty} \frac{(m_{HD})_i}{(\mu_{HD})_i i!}\right. \\ &\cdot \left(\frac{m_{HD}\kappa_{HD}\mu_{HD}}{(m_{HD} + \kappa_{HD}\mu_{HD})m_{HD}}\right)^i \times (\mu_{HD} + i - 1)! \\ &\left.\cdot \left\{1 - \sum_{s=0}^{\mu_{HD}+i-1} \frac{\varphi_2^{\,s}}{s!}\left[\frac{(1 + \kappa_{HD})\mu_{HD}}{\psi_{HD}}\right]^s \exp\left(-\frac{(1 + \kappa_{HD})\mu_{HD}}{\psi_{HD}}\varphi_2\right)\right\}\right\}. \end{aligned} \tag{37}$$

Substitute the obtained I_1 and I_2 into (33), and finally, acquire (25). Moreover, we can obtain the ideal expression of OP in (26) by setting $f_{BH} = f_{HD} = 0$ and $\sigma_{e_{BH}}^2 = \kappa_{e_{HD}}^2 = 0$.

B. The Proof of Theorem 2

B.1. Nonideal Situation

(1) When $\sigma_{e_{XY}}^2 = \Omega/(1+\delta\rho\Omega)$

When seeking the approximation of high SNR, we can employ a similar method to [47] to obtain the following expression for the CDF of the channel gain of the κ-μ shadowed fading as

$$F_{|\hat{h}_{XY}|^2}(x) = \left(\frac{m_{XY}+\kappa_{XY}\mu_{XY}}{m_{XY}}\right)^{-m_{XY}} \frac{1}{\Gamma(\mu_{XY})} \sum_{i=1}^{\infty} \frac{(m_{XY})_i}{(\mu_{XY})_i i!} \cdot \left(\frac{m_{XY}\kappa_{XY}\mu_{XY}}{(m_{XY}+\kappa_{XY}\mu_{XY})m_{XY}}\right)^{i} \times \frac{1}{(\mu_{XY}+i)} \cdot \left(\frac{(1+\kappa_{XY})\mu_{XY}}{\psi_{XY}}x\right)^{\mu_{XY}+i} \exp\left(-\frac{(1+\kappa_{XY})\mu_{XY}}{\psi_{XY}}x\right). \tag{38}$$

According to (38), we can get the approximate expression (39) of the CDF as

$$F_{|\hat{h}_{BH}|^2}^{\infty,\mathrm{ni}}(x) = \left\{\left(\frac{m_{BH}+\kappa_{BH}\mu_{BH}}{m_{BH}}\right)^{-m_{BH}} \frac{1}{\Gamma(\mu_{BH})} \cdot \sum_{i=1}^{\infty}\left(\frac{m_{BH}\kappa_{BH}\mu_{BH}}{(m_{BH}+\kappa_{BH}\mu_{BH})m_{BH}}\right)^{i} \times \frac{1}{(\mu_{BH}+i)}\frac{(m_{BH})_i}{(\mu_{BH})_i i!} \cdot \left(\frac{(1+\kappa_{BH})\mu_{BH}}{\psi_{BH}}x\right)^{\mu_{BH}+i} \exp\left(-\frac{(1+\kappa_{BH})\mu_{BH}}{\psi_{BH}}x\right)\right\}^{L}. \tag{39}$$

Similar to the method in Appendix A, the expressions of I_1 and I_2 can be written as

$$I_3 = F_{|\hat{h}_{BH}|^2}^{\infty,\mathrm{ni}}(\varphi_1) = \left\{\left(\frac{m_{BH}+\kappa_{BH}\mu_{BH}}{m_{BH}}\right)^{-m_{BH}} \frac{1}{\Gamma(\mu_{BH})}\sum_{i=1}^{\infty}\left(\frac{m_{BH}\kappa_{BH}\mu_{BH}}{(m_{BH}+\kappa_{BH}\mu_{BH})m_{BH}}\right)^{i} \cdot \times \frac{1}{(\mu_{BH}+i)}\frac{(m_{BH})_i}{(\mu_{BH})_i i!}\left(\frac{(1+\kappa_{BH})\mu_{BH}}{\psi_{BH}}\varphi_1\right)^{\mu_{BH}+i} \exp\left(-\frac{(1+\kappa_{BH})\mu_{BH}}{\psi_{BH}}\varphi_1\right)\right\}^{L}, \tag{40}$$

$$I_4 = F_{|\hat{h}_{HD}|^2}^{\infty,\mathrm{ni}}(\varphi_2) = \left(\frac{m_{HD}+\kappa_{HD}\mu_{HD}}{m_{HD}}\right)^{-m_{HD}} \frac{1}{\Gamma(\mu_{HD})}\sum_{i=1}^{\infty}\left(\frac{m_{HD}\kappa_{HD}\mu_{HD}}{(m_{HD}+\kappa_{HD}\mu_{HD})m_{HD}}\right)^{i} \cdot \times \frac{1}{(\mu_{HD}+i)}\frac{(m_{HD})_i}{(\mu_{HD})_i i!}\left(\frac{(1+\kappa_{HD})\mu_{HD}}{\psi_{HD}}\varphi_2\right)^{\mu_{HD}+i} \exp\left(-\frac{(1+\kappa_{HD})\mu_{HD}}{\psi_{HD}}\varphi_2\right). \tag{41}$$

In summary, we can get the approximate expression of OP at high SNR as

$$P_{\mathrm{out}}^{\infty,\mathrm{ni}1} = I_3 + I_4 - I_3 I_4. \tag{42}$$

(2) When $\sigma_{e_{XY}}^2 = a$ (a is a fixed value)

When we set $P_J = P_R/2$, the expressions of $B \longrightarrow H$ and $H \longrightarrow D$ channel capacity under high SNR are deduced as

$$C_{BH}^{\infty,\mathrm{ni}} = \frac{1}{2}\log_2\left(1 + \frac{\left|\hat{h}_{BH}\right|^2}{\sigma_{e_{BH}}^2 + f_{BH}^2\left(\left|\hat{h}_{BH}\right|^2 + \sigma_{e_{BH}}^2\right)}\right), \tag{43}$$

$$C_{HD}^{\infty,\mathrm{ni}} = \frac{1}{2}\log_2\left(1 + \frac{\left|\hat{h}_{HD}\right|^2}{\sigma_{e_{HD}}^2 + \left(\xi_1/2 + f_{HD}^2\right)\left(\left|\hat{h}_{HD}\right|^2 + \sigma_{e_{HD}}^2\right)}\right). \tag{44}$$

Combined with the method in Appendix A, the formula of OP at high SNR can be obtained as

$$P_{\mathrm{out}}^{\infty,\mathrm{ni}2} = \Pr\left\{\min\left(C_{BH}^{\infty,\mathrm{ni}}, C_{HD}^{\infty,\mathrm{ni}}\right) < Rs\right\} = \Pr\left\{C_{BH}^{\infty,\mathrm{ni}} < Rs\right\} + \Pr\left\{C_{HD}^{\infty,\mathrm{ni}} < Rs\right\} - \Pr\left\{C_{BH}^{\infty,\mathrm{ni}} < Rs\right\}\Pr\left\{C_{HD}^{\infty,\mathrm{ni}} < Rs\right\} = I_5 + I_6 - I_5 I_6, \tag{45}$$

where I_5 and I_6 are, respectively, expressed as

$$I_5 = \Pr\left\{\left|\hat{h}_{BH}\right|^2 < \varphi_7\right\} = \left\{\left(\frac{m_{BH}+\kappa_{BH}\mu_{BH}}{m_{BH}}\right)^{-m_{BH}} \frac{1}{\Gamma(\mu_{BH})} \cdot \sum_{i=1}^{\infty}\left(\frac{m_{BH}\kappa_{BH}\mu_{BH}}{(m_{BH}+\kappa_{BH}\mu_{BH})m_{BH}}\right)^{i} \times (\mu_{BH}+i-1)!\frac{(m_{BH})_i}{(\mu_{BH})_i i!} \cdot \left\{1 - \sum_{s=0}^{\mu+i-1}\frac{\varphi_7^{\,s}}{s!}\left[\frac{(1+\kappa_{BH})\mu_{BH}}{\varphi_7}\right]^{s}\exp\left(-\frac{(1+\kappa_{BH})\mu_{BH}}{\varphi_7}\varphi_7\right)\right\}\right\}^{L}, \tag{46}$$

$$I_6 = \left(\frac{m_{HD}+\kappa_{HD}\mu_{HD}}{m_{HD}}\right)^{-m_{HD}} \frac{1}{\Gamma(\mu_{HD})}\sum_{i=1}^{\infty}\frac{(m_{HD})_i}{(\mu_{HD})_i i!}\left(\frac{m_{HD}\kappa_{HD}\mu_{HD}}{(m_{HD}+\kappa_{HD}\mu_{HD})m_{HD}}\right)^{i} \times (\mu_{HD}+i-1)!\left\{1 - \sum_{s=0}^{\mu_{HD}+i-1}\frac{\varphi_8^{\,s}}{s!}\left[\frac{(1+\kappa_{HD})\mu_{HD}}{\varphi_8}\right]^{s}\exp\left(-\frac{(1+\kappa_{HD})\mu_{HD}}{\varphi_8}\varphi_8\right)\right\}, \tag{47}$$

where $\varphi_7 = ((\Theta\sigma_{e_{BH}}^2(1+f_{BH}^2))/(1-\Theta f_{BH}^2))$, $\varphi_8 = ((\Theta\sigma_{e_{HD}}^2(1+\xi_1/2+f_{HD}^2))/(1-\Theta\xi_1/2-\Theta f_{HD}^2))$. By substituting the calculated I_5 and I_6 into (45), the precise expression (31) of the OP under high SNR can be obtained.

B.2. Ideal Situation. When $\sigma_{e_{XY}}^2 = \Omega_{XY}/(1+\delta\rho_{XY}\Omega_{XY})$, the high SNR of OP under ideal case can be approximated as

$$I_7 = \left\{\left(\frac{m_{BH}+\kappa_{BH}\mu_{BH}}{m_{BH}}\right)^{-m_{BH}} \frac{1}{\Gamma(\mu_{BH})}\sum_{i=1}^{\infty}\frac{(m_{BH})_i}{(\mu_{BH})_i i!}\left(\frac{m_{BH}\kappa_{BH}\mu_{BH}}{(m_{BH}+\kappa_{BH}\mu_{BH})m_{BH}}\right)^{i} \times \frac{1}{(\mu_{BH}+i)}\left(\frac{(1+\kappa_{BH})\mu_{BH}}{\psi_{BH}}\varphi_3\right)^{\mu_{BH}+i}\exp\left(-\frac{(1+\kappa_{BH})\mu_{BH}}{\psi_{BH}}\varphi_3\right)\right\}^{L}, \tag{48}$$

$$I_8 = \left(\frac{m_{HD}+\kappa_{HD}\mu_{HD}}{m_{HD}}\right)^{-m_{HD}} \frac{1}{\Gamma(\mu_{HD})}\sum_{i=1}^{\infty}\frac{(m_{HD})_i}{(\mu_{HD})_i i!} \cdot \left(\frac{m_{HD}\kappa_{HD}\mu_{HD}}{(m_{HD}+\kappa_{HD}\mu_{HD})m_{HD}}\right)^{i} \times \frac{1}{(\mu_{HD}+i)} \cdot \left(\frac{(1+\kappa_{HD})\mu_{HD}}{\psi_{HD}}\varphi_4\right)^{\mu_{HD}+i}\exp\left(-\frac{(1+\kappa_{HD})\mu_{HD}}{\psi_{HD}}\varphi_4\right), \tag{49}$$

$$P_{\text{out}}^{\infty,\text{id}} = I_7 + I_8 - I_7 I_8. \tag{50}$$

Data Availability

The data used to support the findings of this study are available from the corresponding author upon request.

Conflicts of Interest

The authors declare that there is no conflict of interest about the publication of this paper.

Acknowledgments

This work was supported in part by the Key Scientific Research Projects of Higher Education Institutions in Henan Province under Grant 20A510007 and in part by the Doctoral Fund of Henan Polytechnic University under Grant B2022-13.

References

[1] A. D. Wyner, "The wire-tap channel," *The Bell System Technical Journal*, vol. 54, no. 8, pp. 1355–1387, 1975.

[2] N. Yang, L. Wang, G. Geraci, M. Elkashlan, J. Yuan, and M. Di Renzo, "Safeguarding 5G wireless communication networks using physical layer security," *IEEE Communications Magazine*, vol. 53, no. 4, pp. 20–27, 2015.

[3] A. Li, "Enhancing the physical layer security of cooperative NOMA system," in *In 2019 IEEE 3rd information technology, networking, Electronic and Automation Control Conference (ITNEC)*, pp. 2194–2198, Chengdu, China, 2019.

[4] Y. Yao, "Adaptive relay selection with physical layer security for green communications," in *In 2020 IEEE/CIC International Conference on Communications in China (ICCC)*, pp. 1174–1178, Chongqing, China, 2020.

[5] J.-H. Lee, "Full-duplex relay for enhancing physical layer security in multi-hop relaying systems," *IEEE Communications Letters*, vol. 19, no. 4, pp. 525–528, 2015.

[6] F. Zhu and M. Yao, "Improving physical-layer security for CRNs using SINR-based cooperative beamforming," *IEEE Transactions on Vehicular Technology*, vol. 65, no. 3, pp. 1835–1841, 2016.

[7] J. Barros and M. R. D. Rodrigues, "Secrecy capacity of wireless channels," in *In 2006 IEEE International Symposium on Information Theory*, pp. 356–360, Seattle, WA, USA, 2006.

[8] L. Liang, D. Wei, and M. Li, "Wireless physical layer security based on channel pre-compensation for PolSK modulated systems," in *In 2017 IEEE 9th International Conference on Communication Software and Networks (ICCSN)*, pp. 357–361, Guangzhou, China, 2017.

[9] L. Fan, X. Lei, T. Q. Duong, M. Elkashlan, and G. K. Karagiannidis, "Secure multiuser communications in multiple amplify-and-forward relay networks," *IEEE Transactions on Communications*, vol. 62, no. 9, pp. 3299–3310, 2014.

[10] P. K. Gopala, L. Lai, and H. El Gamal, "On the secrecy capacity of fading channels," *IEEE Transactions on Information Theory*, vol. 54, no. 10, pp. 4687–4698, 2008.

[11] F. Benkhelifa, A. Tall, Z. Rezki, and M.-S. Alouini, "On the low SNR capacity of MIMO fading channels with imperfect channel state information," *IEEE Transactions on Communications*, vol. 62, no. 6, pp. 1921–1930, 2014.

[12] Y. Zhu, Y. Xin, and P.-Y. Kam, "Outage probability of Rician fading relay channels," *IEEE Transactions on Vehicular Technology*, vol. 57, no. 4, pp. 2648–2652, 2008.

[13] N. Bhargav, S. L. Cotton, and D. E. Simmons, "Secrecy capacity analysis over κ-μ fading channels: theory and applications," *IEEE Transactions on Communications*, vol. 64, no. 7, pp. 3011–3024, 2016.

[14] O. S. Badarneh, D. B. da Costa, M. Benjillali, and M.-S. Alouini, "Selection combining over double α-μ fading channels," *IEEE Transactions on Vehicular Technology*, vol. 69, no. 3, pp. 3444–3448, 2020.

[15] N. Hajri, N. Youssef, and M. Patzold, "A study on the statistical properties of double Hoyt fading channels," in *In 2009 6th International Symposium on Wireless Communication Systems*, pp. 201–205, Siena, Italy, 2009.

[16] R. Singh and M. Rawat, "Outage analysis of double shadowed κ-μ fading channels," in *In 2019 10th International Conference on Computing, Communication and Networking Technologies (ICCCNT)*, pp. 1–4, Kanpur, India, 2019.

[17] D. H. Tashman, W. Hamouda, and I. Dayoub, "Secrecy analysis over cascaded κ-μ fading channels with multiple eavesdroppers," *IEEE Transactions on Vehicular Technology*, vol. 69, no. 8, pp. 8433–8442, 2020.

[18] M. M. Harb and M. F. Al-Mistarihi, "Dual hop differential amplify-and-forward relaying with selection combining cooperative diversity over Nakagami-m fading channels," in *In 2016 8th IEEE International Conference on Communication Software and Networks (ICCSN*, pp. 225–228, Beijing, China, 2016.

[19] K. Eshteiwi, B. Sleim, and G. Kaddoum, "Full duplex of V2V cooperative relaying over cascaded Nakagami-m fading channels," in *In 2020 International symposium on networks, Computers and Communications (ISNCC)*, pp. 1–5, Montreal, QC, Canada, 2020.

[20] S. Majhi, P. Kumar, and Y. Nasser, "Outage performance of opportunistic of OFDM relaying over Rician fading channel," in *In 2016 23rd International Conference on Telecommunications (ICT)*, pp. 1–5, Thessaloniki, Greece, 2016.

[21] S. O. Ata and I. Altunbas, "Relay antenna selection for V2V communications using PLNC over cascaded fading channels," in *In 2015 International Wireless Communications and Mobile Computing Conference (IWCMC)*, pp. 1336–1340, Dubrovnik, Croatia, 2015.

[22] K. Hu, Q. Gao, Z. Wang, and W. Huang, "Outage performance of two-way decode-and-forward relaying over block fading channels," in *In 2017 IEEE 9th International Conference on Communication Software and Networks (ICCSN)*, pp. 51–55, Guangzhou, China, 2017.

[23] X. Zhang, Z. Yan, Y. Gao, and W. Wang, "On the study of outage performance for Cognitive Relay Networks (CRN) with the Nth best-relay selection in Rayleigh-fading channels," *IEEE Wireless Communications Letters*, vol. 2, no. 1, pp. 110–113, 2013.

[24] L. Wu, L. Yang, J. Chen, and M.-S. Alouini, "Physical layer security for cooperative relaying over Generalized-K fading channels," *IEEE Wireless Communications Letters*, vol. 7, no. 4, pp. 606–609, 2018.

[25] S. Solanki, P. K. Sharma, P. K. Upadhyay, D. B. da Costa, P. S. Bithas, and A. G. Kanatas, "Cognitive multi-relay networks

with RF hardware impairments and channel estimation errors," in *In GLOBECOM 2017 - 2017 IEEE Global Communications Conference*, pp. 1–6, Singapore, 2017.

[26] X. Li, Q. Wang, M. Liu et al., "Cooperative wireless-powered NOMA relaying for B5G IoT networks with hardware impairments and channel estimation errors," *IEEE Internet of Things Journal*, vol. 8, no. 7, pp. 5453–5467, 2021.

[27] X. Li, M. Zhao, M. Zeng et al., "Hardware impaired ambient backscatter NOMA systems: reliability and security," *IEEE Transactions on Communications*, vol. 69, no. 4, pp. 2723–2736, 2021.

[28] S. Solanki, P. K. Upadhyay, D. B. da Costa, P. S. Bithas, A. G. Kanatas, and U. S. Dias, "Joint impact of RF hardware impairments and channel estimation errors in spectrum sharing multiple-relay networks," *IEEE Transactions on Communications*, vol. 66, no. 9, pp. 3809–3824, 2018.

[29] X. Li, M. Liu, C. Deng et al., "Joint effects of residual hardware impairments and channel estimation errors on SWIPT assisted cooperative NOMA networks," *IEEE Access*, vol. 7, pp. 135499–135513, 2019.

[30] M. Toka and O. Kucur, "Performance of MRT/RAS MIMO-NOMA with residual hardware impairments," *IEEE Wireless Communications Letters*, vol. 10, no. 5, pp. 1071–1074, 2021.

[31] X. Li, M. Huang, C. Zhang et al., "Security and reliability performance analysis of cooperative multi-relay systems with nonlinear energy harvesters and hardware impairments," *IEEE Access*, vol. 7, pp. 102644–102661, 2019.

[32] J. F. Paris, "Statistical characterization of κ-μ shadowed fading," *IEEE Transactions on Vehicular Technology*, vol. 63, no. 2, pp. 518–526, 2014.

[33] A. S. M. Badrudduza, S. M. S. Shahriyer, M. K. Kundu, and S. Shabab, "Enhancement of secrecy multicast capacity over κ-μ shadowed fading channel," in *In 2019 IEEE International Conference on Telecommunications and Photonics (ICTP)*, pp. 1–4, Dhaka, Bangladesh, 2019.

[34] J. Sun, H. Bie, and X. Li, "Security performance analysis of SIMO relay systems over composite fading channels," *KSII Transactions on Internet and Information Systems*, vol. 14, no. 6, pp. 1–6, 2020.

[35] M. S. Aloqlah, I. E. Atawi, and M. F. Al-Mistarihi, "On the performance of fixed-gain amplify-and-forward dual-hop relay systems with beamforming under κ-μ shadowed fading," in *In 2015 IEEE 26th Annual International Symposium on Personal, Indoor, and Mobile Radio Communications (PIMRC*, pp. 814–818, Hong Kong, China, 2015.

[36] E. Illi, F. E. Bouanani, and F. Ayoub, "Performance analysis of dual-hop underwater communication system subject to κ-μ shadowed fading channel," in *In 2016 International Conference on Advanced Communication Systems and Information Security (ACOSIS)*, pp. 1–6, Marrakesh, Morocco, 2016.

[37] R. H. Shaik and R. K. Naidu, "Performance evaluation of dual-hop amplify-and-forward scheme over κ–μ shadowed fading channels," *Physical Communication*, vol. 33, pp. 206–214, 2019.

[38] S. Furrer and D. Dahlhaus, "Multiple-antenna signaling over fading channels with estimated channel state information: capacity analysis," *IEEE Transactions on Information Theory*, vol. 53, no. 6, pp. 2028–2043, 2007.

[39] C. W. R. Chiong, Y. Rong, and Y. Xiang, "Blind estimation of MIMO relay channels," in *2014 IEEE Workshop on Statistical Signal Processing (SSP)*, pp. 400–403, Gold Coast, QLD, Australia, 2014.

[40] N. Missaoui, I. Kammoun, and M. Siala, "Efficient user identification and semi-blind channel estimation for MU-MIMO systems," *IEEE Wireless Communications Letters*, vol. 6, no. 2, pp. 150–153, 2017.

[41] X. Li, J. Li, Y. Liu, Z. Ding, and A. Nallanathan, "Outage performance of cooperative NOMA networks with hardware impairments," in *In 2018 IEEE Global Communications Conference (GLOBECOM)*, pp. 1–6, Abu Dhabi, United Arab Emirates, 2018.

[42] X. Ding, T. Song, Y. Zou, X. Chen, and L. Hanzo, "Security-reliability tradeoff analysis of artificial noise aided two-way opportunistic relay selection," *IEEE Transactions on Vehicular Technology*, vol. 66, no. 5, pp. 3930–3941, 2017.

[43] F. Gabry, R. Thobaben, and M. Skoglund, "Outage performances for amplify-and-forward, decode-and-forward and cooperative jamming strategies for the wiretap channel," in *In 2011 IEEE Wireless Communications and Networking Conference*, pp. 1328–1333, Cancun, Mexico, 2011.

[44] L. Peng, G. Zang, Q. Zhou, Y. Gao, and C. Xi, "Security performance analysis for cooperative communication system under Nakagami-m fading channel," in *In 2017 IEEE 17th International Conference on Communication Technology (ICCT)*, pp. 187–192, Chengdu, China, 2017.

[45] E. Bjornson, M. Matthaiou, and M. Debbah, "A new look at dual-hop relaying: performance limits with hardware impairments," *IEEE Transactions on Communications*, vol. 61, no. 11, pp. 4512–4525, 2013.

[46] V. Kumar, B. Cardiff, S. Prakriya, and M. F. Flanagan, "Effective rate of downlink NOMA over κ-μ shadowed fading with integer fading parameters," in *In 2020 IEEE International Conference on Communications Workshops (ICC Workshops)*, pp. 1–7, Dublin, Ireland, 2020.

[47] J. Sun, H. Bie, X. Li, J. Zhang, G. Pan, and K. M. Rabie, "Secrecy performance analysis of SIMO systems over correlated κ-μ shadowed fading channels," *IEEE Access*, vol. 7, pp. 86090–86101, 2019.